NUMERICAL MODELLING OF PLASMA GENERATION IN A HOLLOW CATHODE TRIGGERED DISCHARGE

A.V. BEREZIN[*], A.S.VORONTSOV[*], M.B. MARKOV[*],

S.V. PAROTKIN[*], S.V. ZAKHAROV[†]

[*] Keldysh Institute of Applied Mathematics (RAS)
Moscow, Russia
e-mail: m_b_markov@mail.ru

[†] EPPRA (European Pulsed Power Research Applications) SaS,
Courtaboeuf, France

Summary: The mathematical model of plasma generation in a gaseous discharge is represented. Model is developed on the base of kinetic equation for electrons in self-consistent electromagnetic field. Elastic scattering of electrons, excitation by the electron impact and impact ionization of molecule are taken into account. The natural ionization background is considered as initial free electrons distribution. The artificial nonreflecting boundary conditions for Maxwell equations are used. The model is verified by the comparison with drift velocity, average energy and Townsend coefficient in charged plane capacitor measured data. The results of plasma generation modeling in a charged capillary EUV-source of a considered design are represented.

1 INTRODUCTION

An electrical discharge in the gaseous medium is an interesting physical object both from scientific and industrial points of view. For instance, physical processes in discharge-produced plasma (DPP) source are of great interest for the development of the sources [1] for the extreme ultraviolet (EUV) lithography application. Determining physical conditions, required for discharge ignition in EUV-source of real design, is not a simple problem. Miniaturization of the sources makes any measurements difficult. The problems of theoretical analysis are connected with complexity of quantitative description for gas discharge in strongly non-uniform electric field, which distinguishes industrial EUV sources from laboratory ones.

This paper represents an attempt to identify the conditions of the discharge ignition in prospective EUV source of a complex design by means of direct mathematical modelling. The image of considered EUV source 3D geometrical model and the coordinate system are shown at Fig. 1.

Cross-section at $z = 1.25$ cm plane.
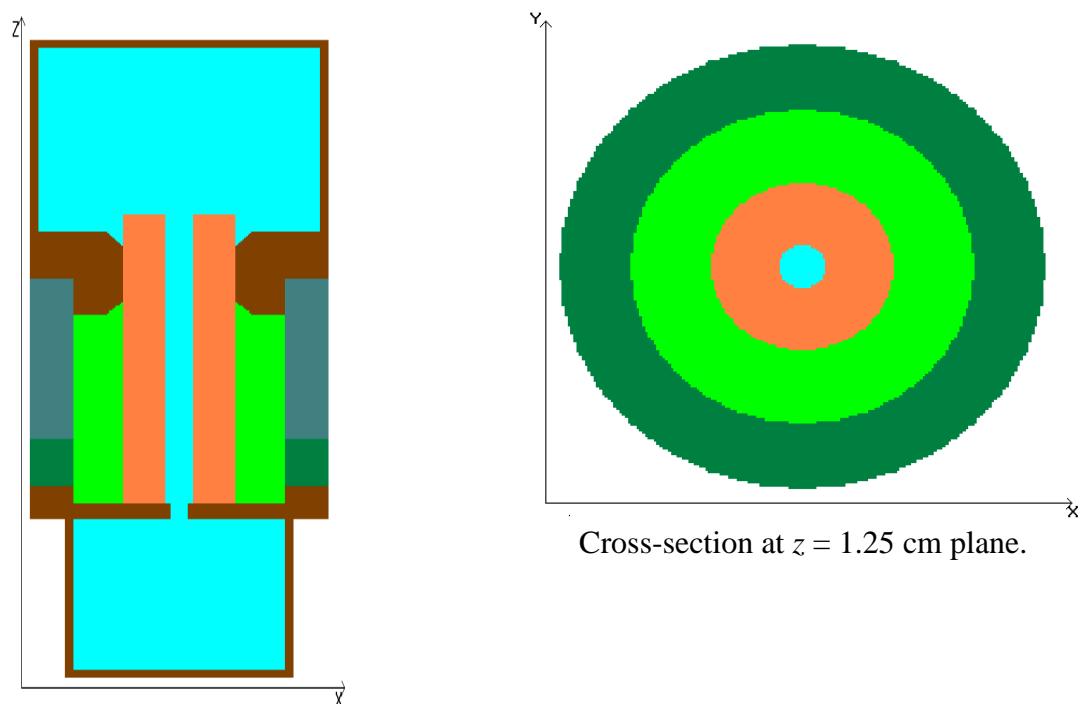
Cross-section at $y = 0$ cm plane

Figure 1: The geometrical model of EUV- source.

EUV-source considered has an axially symmetric design. It consists of metallic volumes (highlighted in brown in Fig. 1). The internal height of lower volume is of 1 cm, the radius is of 0.6 cm. The internal height of the upper volume is of 1.2 cm, the radius is of 0.8 cm. The volumes are connected by a dielectric capillary (orange color in Fig. 1) with dielectric permittivity equal to 8. The length of the capillary is of 1.8 cm, the internal radius is of 0.08 cm, the external radius is of 1.2 cm. Three concentric dielectric rings with dielectric permittivity equal to 1 (light green, dark green and a at Fig. 1b) complete the design. The height of the light green ring is of 1.18-1.25 cm, the internal radius is of 0.32 cm, the external radius is of 0.6 cm. The height of the dark green ring is of 0.3 cm, internal radius is of 0.6 cm, external radius is of 0.85 cm. The height of the sea-wave colored ring is of 0.3 cm, the internal radius is of 0.6 cm, the external radius is of 0.85 cm. The metallic volumes and the capillary are filled by rarified xenon or nitrogen-xenon mixture (blue). The pressure of the gas is equal to 1 Torr in the lower volume and is declines linearly with the height to 0.025 Torr in the capillary, and it is equal to 0.025 Torr in upper volume. It is supposed, that free electrons are distributed uniformly with the density of 10^9 $1/cm^3$ in the gas as the initial ionization background. The discharge development in the electric field is considered on the background of motionless ion and neutral molecule distributions.

Initially free electrons are in the state of heat equilibrium with gas molecules. The electron energy of heat equilibrium averages 0.04 eV. When external electric field is switched on the initial energy of electrons begins to increase due to acceleration electromagnetic field forces. The scattering on gas molecules attempts to reduce the motion anisotropy of accelerated electron. The energy of electron directed motion turns into the heat energy. The energy, that electron transfers to molecule during the elastic collision, is approximately proportional to their mass ratio. Thus, as far as this ratio is small and elastic scattering at small energies prevails over other collisions the electron temperature begins to increase.

The heating rate begins to decrease when electron temperature attains the threshold of molecule excitation. The excitation threshold for xenon is approximately of 8 eV. The further heating leads to attainment of ionization threshold. The ionization threshold for xenon is approximately of 12.13 eV. The process of ionization scattering becomes essential above this temperature level. Ionization scattering results in increased amount of free electrons.

The further temperature dynamics depends on the gas density and the electric field strength. The equilibrium between the field and collisions can be reached in a dense gas. It means that in average the electrons loose in collisions the same energy that they receive from the field between inelastic interactions. When the electric field strength is high and the gas is rarefied enough, a free electron can be accelerated by electric field from soft spectral region to hard one during his lifetime between collisions. In this case electron can skip peak region of inelastic cross-section (50 eV). It would result in the further increase of its energy and in the decrease of the ionization rate. In this case a run-away electron beam can be formed.

A mathematical description and a quantitative analysis of mentioned processes by means of mathematical modeling is the subject of this paper.

2 MATHEMATICAL MODEL FOUNDATIONS

The dynamics of electrons in weekly-ionized EUV-source gaseous medium is described by 3D kinetic and electrodynamics equations. The distribution function $f \equiv f(t,\mathbf{r},\mathbf{p})$ defines the electron density in the phase space $(\mathbf{r},\mathbf{p}) = \mathbb{R}^3_\mathbf{r} \times \mathbb{R}^3_\mathbf{p}$ of coordinates $\mathbf{r}$ and momentums $\mathbf{p}$. The following kinetic equation is used:

$$\frac{\partial f}{\partial t} + \operatorname{div}_\mathbf{r}(\mathbf{v}f) - e\frac{\partial}{\partial \mathbf{p}}\left[\left(\mathbf{E}+[\boldsymbol{\beta},\mathbf{H}]\right)f\right] + \sigma_t vf = Q(\mathbf{p}) + \int d\mathbf{p}'\sigma(\mathbf{p},\mathbf{p}')v'f(\mathbf{p}') \qquad (1)$$

Here t means laboratory time, e – electron charge, $\mathbf{v}$ – electron speed, $\boldsymbol{\beta} = \mathbf{v}/c$, $\mathbf{E} = \mathbf{E}(t,\mathbf{r})$, $\mathbf{H} = \mathbf{H}(t,\mathbf{r})$ are electric and magnetic field strengths. The given function $Q \equiv Q(t,\mathbf{r},\mathbf{p})$ in the phase space describes the continuous spectrum electron generation. Tree types of electron collisions with neutral molecules are considered [2]: elastic scattering, molecule excitation and impact ionization. These processes in a weekly-ionized gas are described by the linear collision integral $\sigma_t vf - \int d\mathbf{p}'\sigma(\mathbf{p},\mathbf{p}')v'f(\mathbf{p}')$, where $\sigma_t(p)$ is the total macroscopic cross-section of the electron absorption (scattering), $\sigma(\mathbf{p},\mathbf{p}')$ is the sum of all differential macroscopic cross-sections of the electron scattering. Symbols $\mathbf{p}'$ and $\mathbf{p}$ denote electron momentums before and after collision correspondingly.

Maxwell equations describe the electromagnetic field:

$$\operatorname{rot}\mathbf{H} = \frac{1}{c}\frac{\partial \mathbf{E}}{\partial t} + \frac{4\pi}{c}\mathbf{j}, \ \operatorname{rot}\mathbf{E} = -\frac{1}{c}\frac{\partial \mathbf{H}}{\partial t}, \qquad (2)$$

where $\mathbf{j} \equiv \mathbf{j}(t,\mathbf{r})$ is the electron current density.

The ion distribution is generated simultaneously with electron one and with the same intensity. The ion motion in mathematical model is neglected.

Equations (1-2) with corresponding initial conditions define the Cauchy problem for the system of hyperbolic equations of the first order.

The solution of the equation (1) is constructed by the successive generations method. The solution of the kinetic equation for the zero generation distribution $f_0 \equiv f_0(t,\mathbf{r},\mathbf{p})$ is:

$$f_0 = \int_0^t d\tau \int d\boldsymbol{\xi} \int d\boldsymbol{\eta}\, Q(\tau,\boldsymbol{\xi},\boldsymbol{\eta}) \exp\left\{-\int_\tau^t dt''\sigma_t v\left(p^s(t'')\right)\right\} \delta(\mathbf{r}-\mathbf{r}^s)\delta(\mathbf{p}-\mathbf{p}^s)$$

where $\tau,\boldsymbol{\xi},\boldsymbol{\eta}$ are variables of integration. Functions $\mathbf{r}^s(t,\tau,\boldsymbol{\xi},\boldsymbol{\eta})$, $\mathbf{p}^s(t,\tau,\boldsymbol{\xi},\boldsymbol{\eta})$ are the solutions of motion equations $d\mathbf{r}^s/dt = \mathbf{v}^s$, $d\mathbf{p}^s/dt = \mathbf{E}(t,\mathbf{r}^s,\mathbf{p}^s)+\left[\boldsymbol{\beta}^s,\mathbf{H}(t,\mathbf{r}^s,\mathbf{p}^s)\right]$ with initial data $\mathbf{r}^s\big|_{t=\tau}=\boldsymbol{\xi}$, $\mathbf{p}^s\big|_{t=\tau}=\boldsymbol{\eta}$.

Distribution f_0 is considered in the space of finite generalized functions [3] defined on infinitely differentiable functions $\varphi = \varphi(\mathbf{r},\mathbf{p})$ with a common support in $\mathbb{R}^3_\mathbf{r} \times \mathbb{R}^3_\mathbf{p}$. The variable t is a parameter. The action of generalized function on the element of pivot space is as follows:

$$(\varphi,f_0) = \int_0^t d\tau \int d\boldsymbol{\xi} \int d\boldsymbol{\eta}\, Q(\tau,\boldsymbol{\xi},\boldsymbol{\eta}) \exp\left\{-\int_\tau^t dt''\sigma_t v\left(p^s(t'')\right)\right\} \varphi(\mathbf{r}^s,\mathbf{p}^s)$$

Let $Q \equiv Q(t,\mathbf{r},\mathbf{p})$ be a sum of elementary sources:

$$Q(t,\mathbf{r},\mathbf{p}) = \sum_k F_k(t)\Theta(t_k+\Delta t_k-t)\Theta(t-t_k)\delta(\mathbf{r}-\mathbf{r}_k)\delta(\mathbf{p}-\mathbf{p}_k). \tag{3}$$

Then

$$f_0 = \sum_k N_k \exp\left\{-\int_{t_k}^t dt''\sigma_t v\left(p^s(t'',t_k,\mathbf{r}_k,\mathbf{p}_k)\right)\right\}\delta(\mathbf{r}-\mathbf{r}^s(t,t_k,\mathbf{r}_k,\mathbf{p}_k))\delta(\mathbf{p}-\mathbf{p}^s(t,t_k,\mathbf{r}_k,\mathbf{p}_k)), \tag{4}$$

where $N_k \equiv \int_{t_k}^{\Delta t_k+t_k} F_k(\tau)d\tau$.

The source of first generation electrons is:

$$\hat{K}f_0 = \sum_k N_k \exp\left\{-\int_{t_k}^t dt''\sigma_t v\left(p_k^{s''}\right)\right\}\delta(\mathbf{r}-\mathbf{r}^s(t,t_k,\mathbf{r}_k,\mathbf{p}_k))\sigma(\mathbf{p},\mathbf{p}^s(t,t_k,\mathbf{r}_k,\mathbf{p}_k)) \tag{5}$$

where $p_k^{s''} \equiv p^s(t'',t_k,\mathbf{r}_k,\mathbf{p}_k)$

Cauchy problem for hyperbolic equations of the first order can be reformulated. Let $f \equiv f(t,\mathbf{r},\mathbf{p})$, $\mathbf{E}=\mathbf{E}(t,\mathbf{r})$, $\mathbf{H}=\mathbf{H}(t,\mathbf{r})$ be the solution of the Cauchy problem considered. One can use these functions as initial conditions for the definition of solution in the time moment $t+\Delta t$. It can be proved, that the sum of zero and first generation distribution functions defines the solution with the first order of accuracy in time, when the condition $\sigma_t v\Delta t \ll 1$ is satisfied. If the distribution function is known on a current time layer, then its calculation on the next time layer with the first order of accuracy requires only the use of zero and first generations of electrons.

One can use the following statistical interpretation [4] of (4), (5):

$$f_0 = \sum_k N_k^e \Theta\left(\exp\left\{-\int_{t_k}^t dt''\sigma_t v\left(p_{0k}^{s''}\right)\right\}-a\right)\delta(\mathbf{r}-\mathbf{r}_k^s(t))\delta(\mathbf{p}-\mathbf{p}_k^s(t)),$$

$$\hat{K}f_0 = \sum_k N_k \delta(\tau_k-(t-t_k))\delta(\mathbf{r}-\mathbf{r}_k^s)\delta(\mathbf{p}-\mathbf{p}_k^1).$$

$$f_1 = \sum_k N_k \Theta(t - t_k - \tau_k) \Theta\left(\exp\left\{-\int_{t_k+\tau_k}^{t} dt'' \sigma_t v\left(p^s\left(t'', t_k + \tau_k, \mathbf{r}_k^s(t_k + \tau_k), \mathbf{p}_k^1\right)\right)\right\} - a_1\right) \times$$

$$\times \delta\left(\mathbf{r} - \mathbf{r}^s\left(t, t_k + \tau_k, \mathbf{r}_k^s(t_k + \tau_k), \mathbf{p}_k^1\right)\right) \delta\left(\mathbf{p} - \mathbf{p}^s\left(t, t_k + \tau_k, \mathbf{r}_k^s(t_k + \tau_k), \mathbf{p}_k^1\right)\right)$$

where independent random variables a and a_1 are distributed uniformly in the interval $[0,1]$, random variable τ_k is the solution of equation $\exp\left\{-\int_{t_k}^{t_k+\tau_k} dt'' \sigma_t v\left(p_k^{s''}\right)\right\} - a$, random variable $\mathbf{p}_k^1$ is distributed with probability density $w\left(\mathbf{p}, \mathbf{p}_k^s\right) \equiv \sigma\left(\mathbf{p}, \mathbf{p}_k^s\right) / \sigma_t\left(p_k^s\right)$.

Current density $\mathbf{j} \equiv \mathbf{j}(t, \mathbf{r})$ in Maxwell equations is defined as the action of generalized function f:

$$\mathbf{j} = e\left(f(t, \boldsymbol{\alpha}, \mathbf{p}), \mathbf{v} W\left(|\mathbf{r} - \boldsymbol{\alpha}|, \Delta\right)\right),$$

where $W\left(|\mathbf{r} - \boldsymbol{\alpha}|, \Delta\right)$, $\boldsymbol{\alpha} \in \, _{\mathbf{r}}^3$, $\Delta > 0$ is infinitely differentiable function on $_{\mathbf{r}}^3$.

The description of the electron distribution in terms of generalized functions with random parameters uses a combination of Monte-Carlo and particles methods for numerical modeling [5].

The numerical solution of motion equations is considered in details in [6]. It distinguishes from other realizations of «cloud-in-cell» model by guaranteed conservation of charge and availability of non uniform computational mesh. Current density in cell edges is calculated through charge change in cell's vertices during time step. Cartesian coordinates are used. System of linear equations in current components is closed up by additional condition: during one time step, the particle direction does not change and coincides with direction of its current. When particle crosses a cell boundary, its motion is to be divided into two steps: before and after intersection. Particles coordinates are calculated by numerical solution of ordinary differential equation with the help of an explicit difference scheme. Centered difference scheme is used for momentum equation numerical solution.

When the time step is done, the probability of absorption $\sigma_t v \Delta t$ is calculated with a new momentum absolute value. A pseudo-random number generator is used to determine if absorption "happened" or not. In this case particle disappears. A new particle is generated with the same coordinates. The momentum of the new particle is sampled randomly from distribution $w\left(\mathbf{p}, \mathbf{p}_k^s(t + \Delta t)\right)$. This algorithm realizes the Poisson stream of events.

Maxwell equations are considered in Cartesian coordinates. The explicit difference scheme is used for numerical solution. Scheme is constructed as approximation of Maxwell equations in the integral form. Computational mesh and finite-difference equations are represented in [7] in details. Difference scheme allows discontinuities in the dielectric and magnetic permittivity, current density and electric conductivity. The scheme applicability is restricted by the Courant condition. If it is satisfied the finite difference solution converges to the exact one. The artificial non-reflecting boundary conditions for Maxwell equations are approved for model considered.

Cross-section data for low energy electrons from different sources are used. The elastic scattering differential cross-sections dependencies on the angle for different electron energies are collected from [8-15]. The corresponding total cross-sections for energies from excitation threshold up to 100 eV are drawn from [16]. The Bethe-Born approach is used for energies, which exceed 100 eV [17]. Semi-empirical model of total and differential cross-sections of ioni-

zation are represented in [18,19]. Semi-empirical model is verified by comparison with experimental data [20,21].

Many experiments confirmed the considered model [22]. One can trust in it, when electron energy exceeds 1 KeV. However, cross-sections for low energy electrons were obtained in a complex and conflicting process. Additional comparison with experimental data on the drift velocity, average energy and Townsend coefficient of the ionization process under electrostatic field in plane capacitor [23-27] indicates that computational results do not contradict to experimental observations.

3   THE RESULTS OF MODELLING

The design, which is described as EUV-source, represents a gas filled diode. Metallic volumes play role of electrodes. Initial distribution of the electric field depends on a simulated geometry. It ia calculated by the setting method. The charging of the diode is modelled by an external electric current inclusion between electrodes. The electric current with density $j_z = A\sin(\pi\omega t)$ is assigned in every cell of the mesh in the range $0 < \sqrt{x^2 + y^2} < 0.85$ cm, $1.2\,\text{cm} < z < 2.5\,\text{cm}$. The capacitor charges up to 23 KV in the course of 10^{-10} s, when $A = 4.1 \cdot 10^{12}$ CGSE, $\omega = 10^{10}$ 1/s.

The Maxwell equations are solved with the described current density in the right-hand side. The calculation shows, that electrostatic field is settled in the course of 50 ns. The distribution of steady-state electrostatic field in xenon is shown in Fig. 2. Regions of the gas, where the electric field is equal to zero are marked by yellow. Regions of the gas, where the electric field is positive are marked by red, negative – by blue.
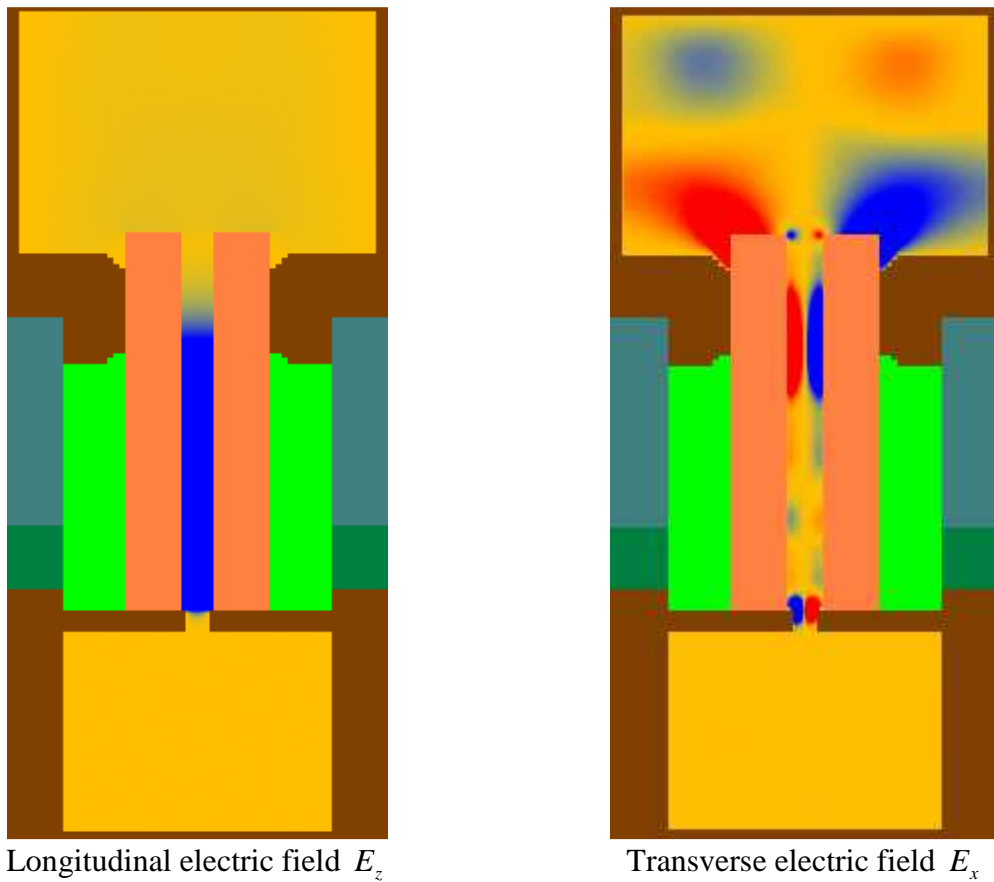
Longitudinal electric field E_z Transverse electric field E_x

Figure 2: The distribution of the steady-state electric field in xenon after power-up.

Longitudinal electric field along the axis of source   Transverse electric field in a section by plane $z = 1.25$ cm
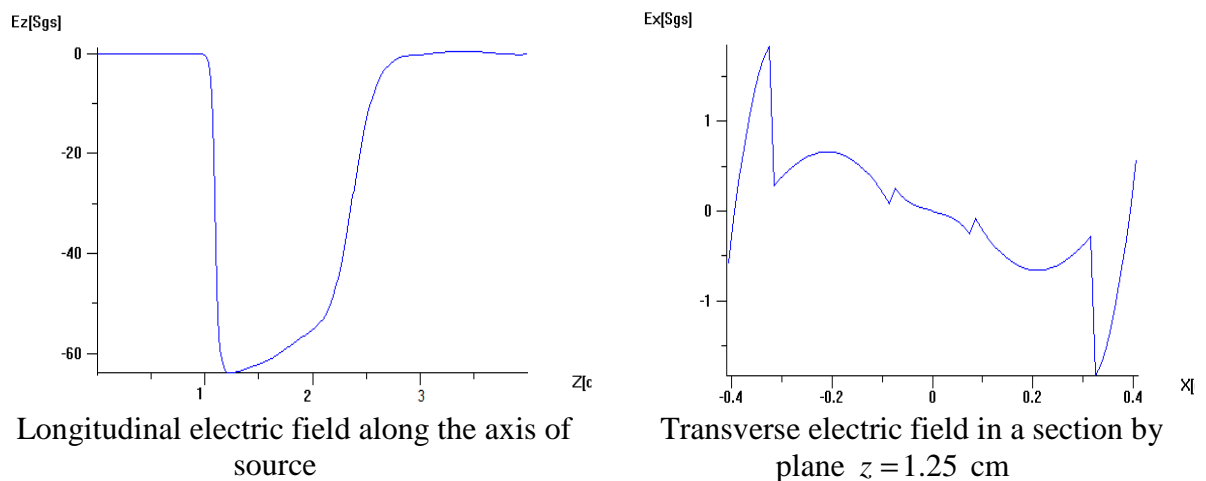
Figure 3: The distribution of the steady-state electric field by coordinates.

The field distribution is calculated at a hybrid cluster computer K-100 in KIAM. Computational mesh contained 13 357 800 spatial cells. Time step is equal to 10^{-13} s.

Discharge starts at the moment when external charge current is switching on. Mathematical model can describe this process, but since we have no exact information about process of charging we are forced to start considering electron motion at the moment when electric field is already established.

Only elastic scattering affects the electron flux when pressure in lower volume is equal to 1 Torr. Free electrons leave the capillary and accumulate near its exit at the upper volume of source. At the same time, free electrons are pulled out from the lower volume by electric field. These electrons are accelerated in capillary without any sufficient inelastic scattering. The electron beam is generated in the capillary. Current strength of the beam reaches 1 A, electron density – 10^{10} 1/cm^3 at capillary axis when $z = 11.6$ cm. The rise of the pressure up to 2 Torr does not change the results of modeling fundamentally.

Changes become visible when the pressure in lower volume increases up to 2.5 Torr. The peak electron density reaches the magnitude of order 10^{11} 1/cm^3 at capillary axis during first 0.5 ns. It is a result of gas ionization by accelerated electrons. The ionization process has one essential feature. The region of the peak electron density appears not near the entrance to the capillary from the lower volume, where gas pressure is maximal and electric field strength is already high, but at a distance of some millimeters from it (Fig. 4 a). The region of the increased electron density is highlighted in red in Fig.4-6, the color scale of the density (1/cm^3) is placed to the right of images. Term "increased" means that the density does not differ considerably from the peak value for the given moment of time. The modeling shows, that the electron beam described above plays an essential role in the formation of the region of increased electron density. The intensive ionization process is not possible without high-energy electrons.

After formation, the region of increased electron density begins to move in the direction of the exit from the capillary. The peak electron density rises and reaches $3.5 \cdot 10^{11}$ 1/cm^3 during of 1 ns. The transverse size of the region of the peak density diminishes.

$t = 50.5\,\text{ns}$,
peak density $1.4 \cdot 10^{11}\,1/\text{cm}^3$

$t = 51\,\text{ns}$,
peak density $1.7 \cdot 10^{11}\,1/\text{cm}^3$

$t = 51.5\,\text{ns}$,
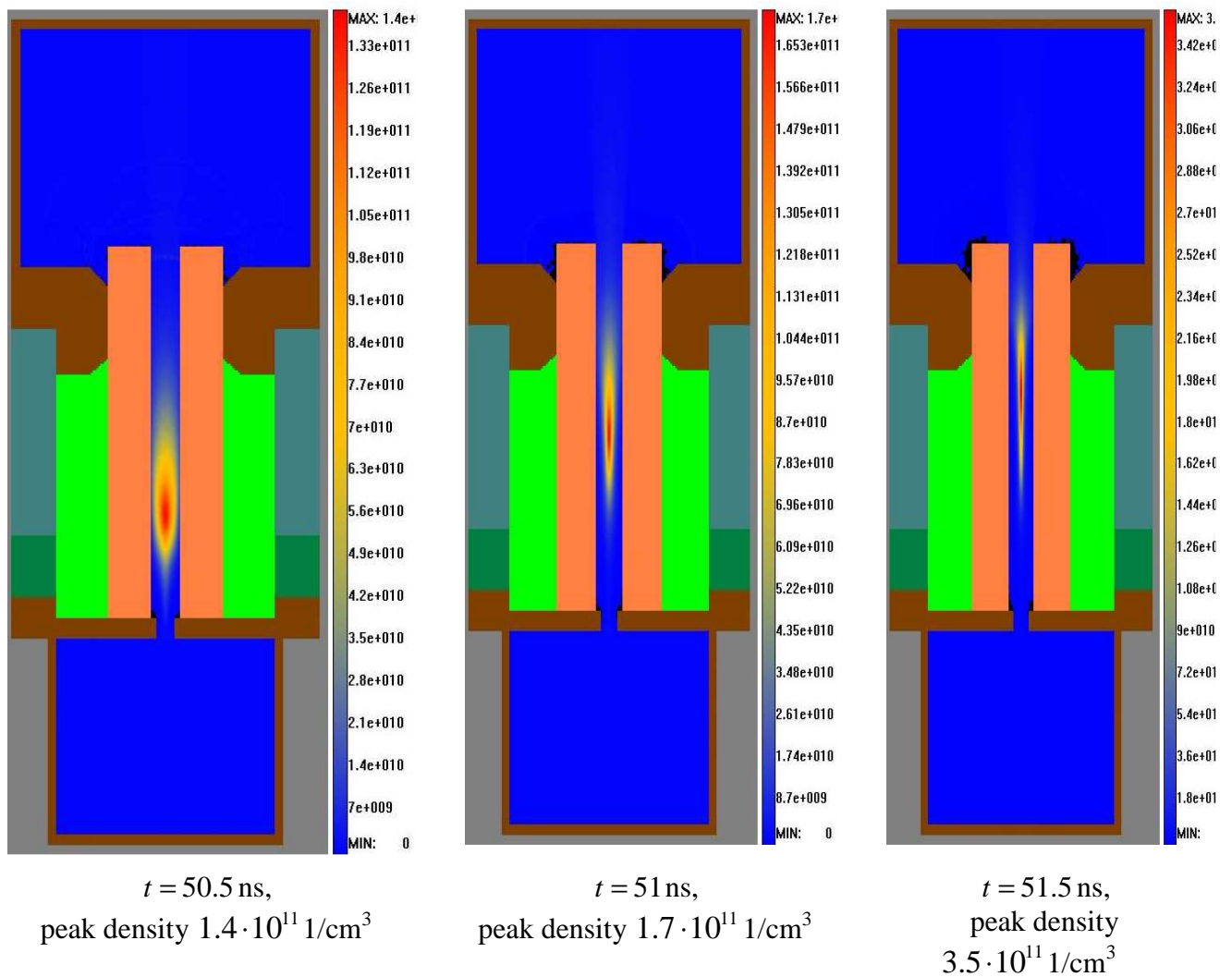peak density
$3.5 \cdot 10^{11}\,1/\text{cm}^3$

Figure 4: The electron density distribution in the capillary, 2.5 Torr at a section $y = 0$ at early stages.

The drift velocity of electron bunch drops dramatically when $t = 52\,\text{ns}$. The peak density continues to rise up to $1.8 \cdot 10^{12}\,1/\text{cm}^3$ (Fig. 5). Then the electron bunch begins to crumble.

$t = 52$ ns,
peak density $4 \cdot 10^{11}$ 1/cm^3

$t = 52.5$ ns,
peak density $7.8 \cdot 10^{11}$ 1/cm^3
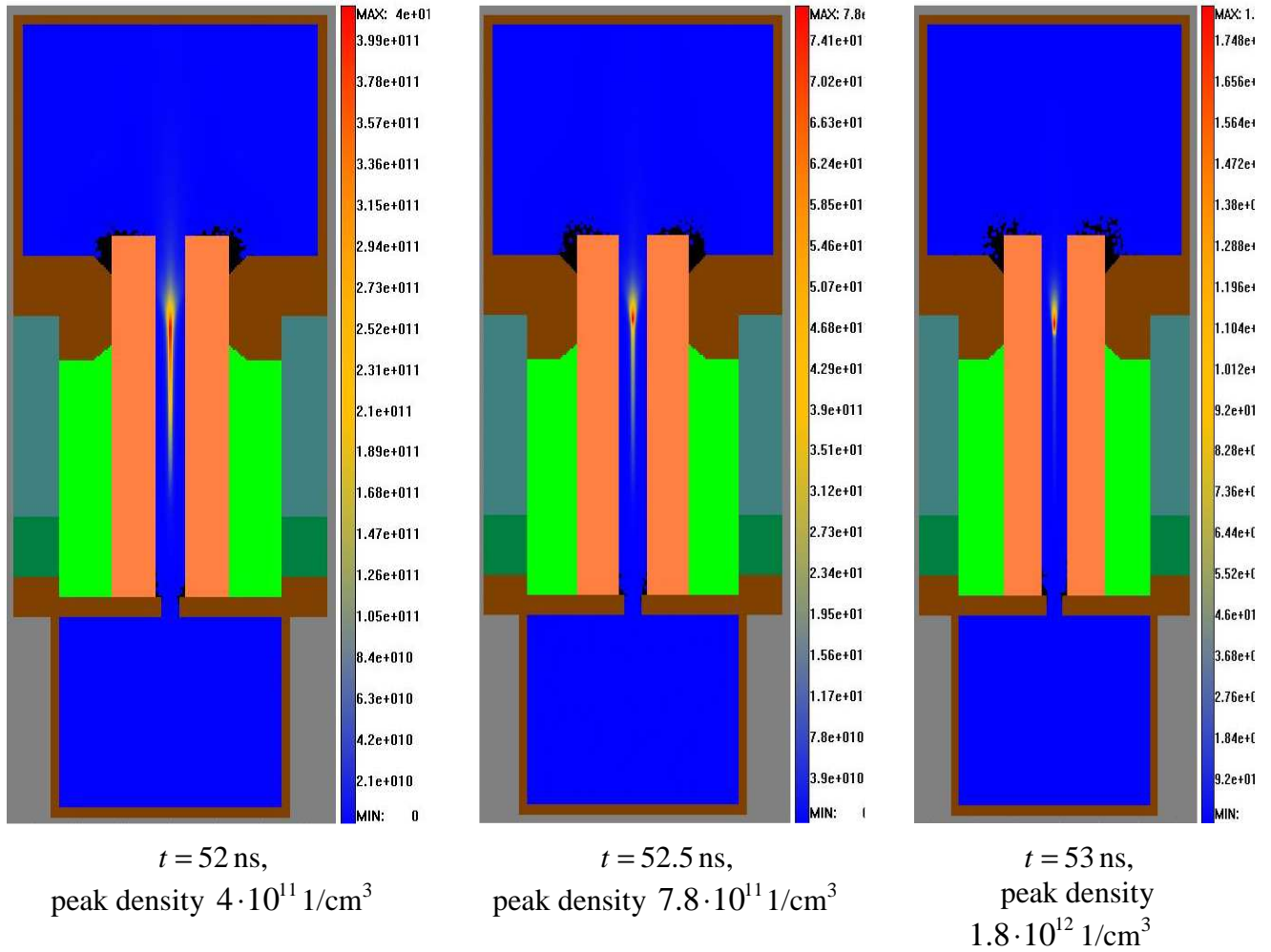
$t = 53$ ns,
peak density
$1.8 \cdot 10^{12}$ 1/cm^3

Figure 5: The electron density distribution in the capillary, 2.5 Torr at a section $y = 0$ at late stages.

The finishing of the ionization process and crumbling of the bunch can be explained by reduction of collision cross-sections along the capillary.

The fundamentally different picture is observed when the value of the pressure reaches 3 Torr, although the region of the increased electron density is forming at the same time and in the same place (Fig. 6).

The shift of the region of increased density is much less, than in the previous case. The density of free electrons increases in the region of high pressure, where collision cross-sections are sufficiently great for the intensive ionization. The peak electron density reaches the size of the order of 10^{12} 1/cm^3 at the same place, where the value of 10^{11} 1/cm^3 is implemented in the previous case.

$t = 50.3\,\text{ns}$,
peak density $2.5 \cdot 10^{10}\,1/\text{cm}^3$

$t = 50.5\,\text{ns}$,
peak density $1.4 \cdot 10^{11}\,1/\text{cm}^3$

$t = 50.7\,\text{ns}$,
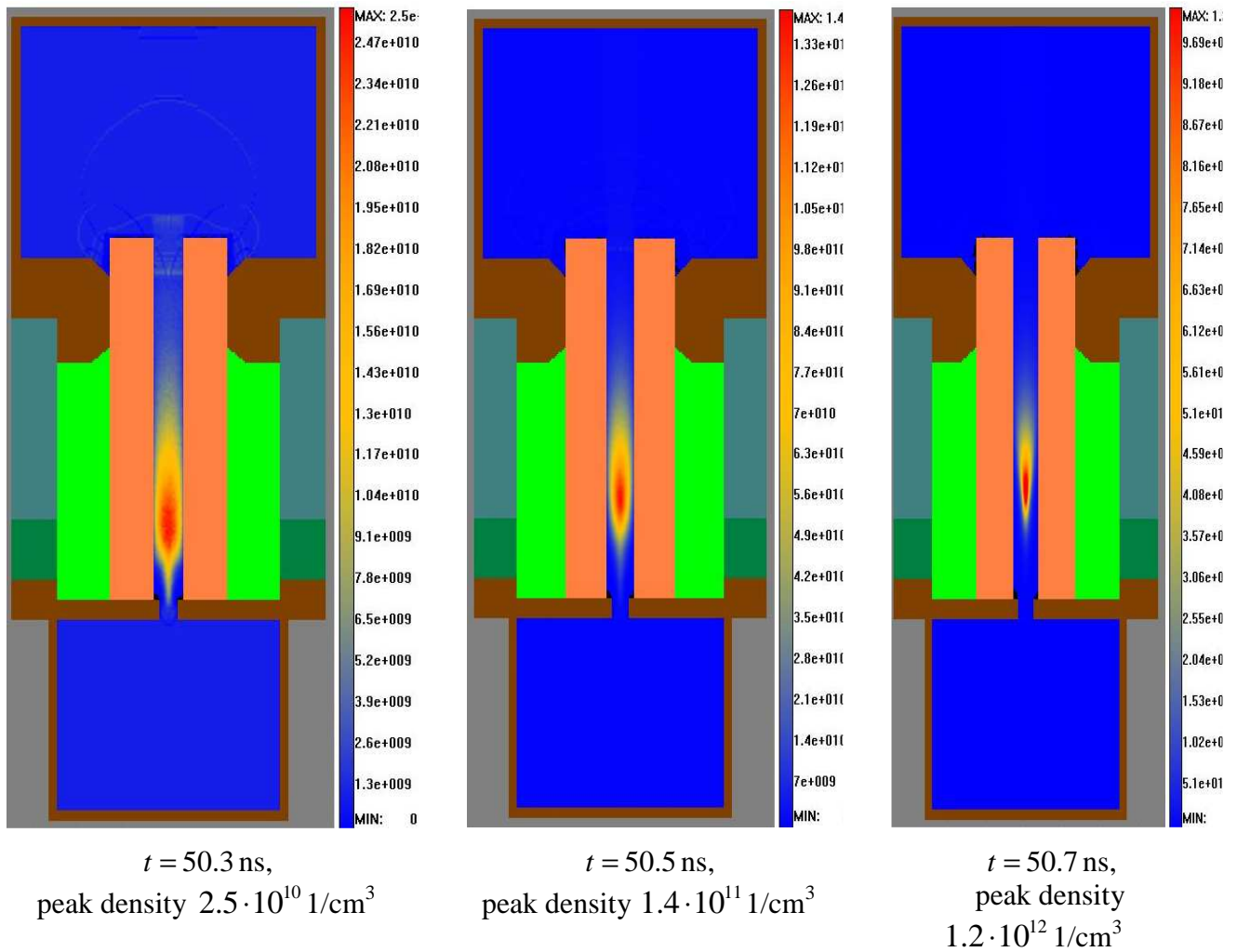peak density
$1.2 \cdot 10^{12}\,1/\text{cm}^3$

Figure 6: The electron density distribution in the capillary at 3 Torr at a section $y = 0$ at early stages.

The subsequent increase of the electron density is accompanied by the compression of the region in which it is forming. The region of the increased density does not drift noticeably (Fig. 7).

The space charge of electrons becomes significant when the electron density reaches the value of $10^{14}\,1/\text{cm}^3$. A reversal electric field is observed. The plasma is generated in a relatively small near axis region inside the capillary in a fixed position.

It is necessary to mention, that the electron beam, which is generated near the entrance of the capillary still plays an important role. Ionization intensity sufficient for the plasma bunch creation isn't possible without high-energy electrons.

The described mathematical model can simulate physical effects of plasma generations, but in order to continue the calculation mesh must be made denser by three orders of magnitude and the time step smaller by one order of magnitude. Moreover, such calculations can require taking into account the movement of ions. This will be the next step of modeling.
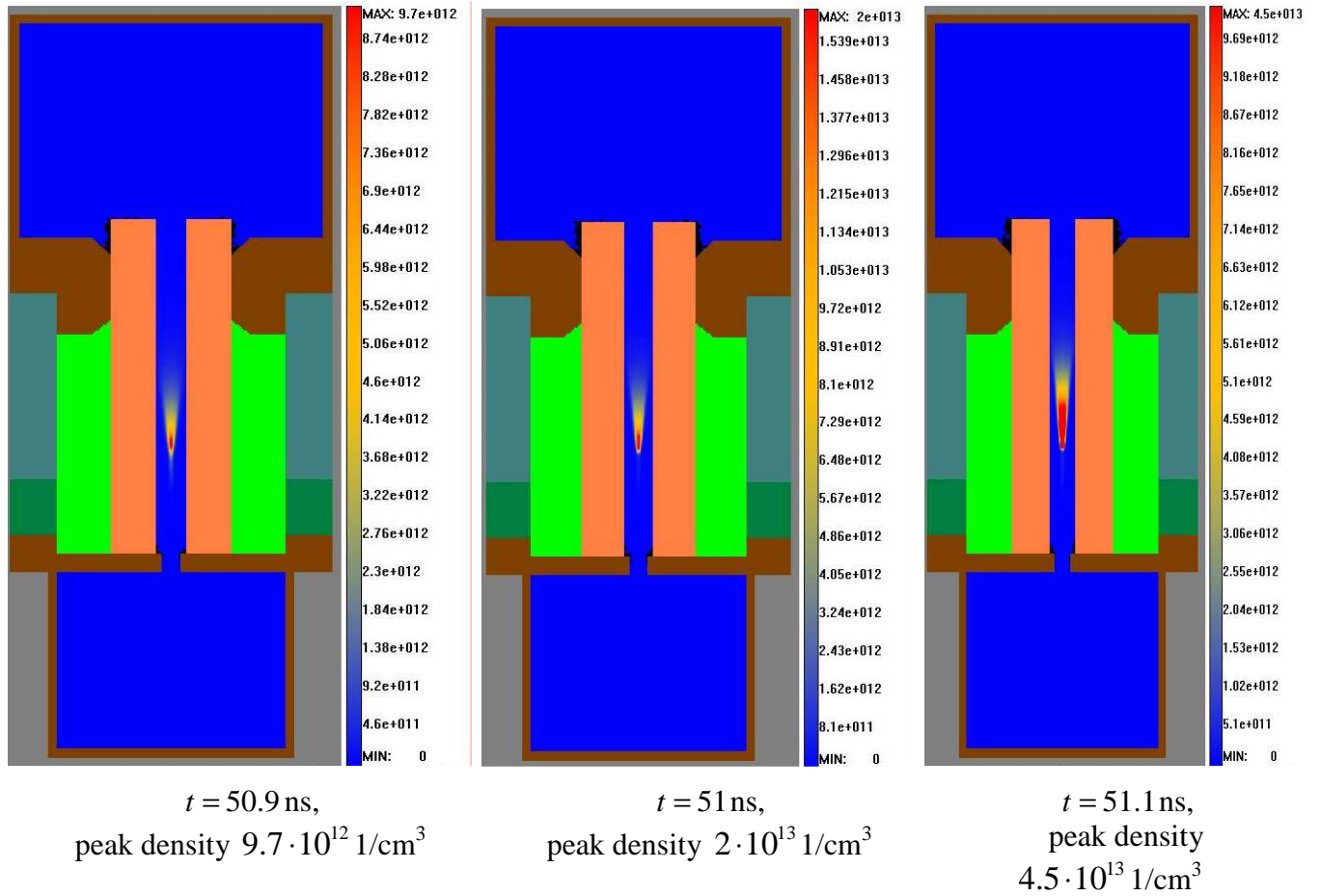
61

$t = 50.9$ ns,	$t = 51$ ns,	$t = 51.1$ ns,
peak density $9.7 \cdot 10^{12}$ 1/cm^3	peak density $2 \cdot 10^{13}$ 1/cm^3	peak density $4.5 \cdot 10^{13}$ 1/cm^3

Figure 7: The electron density distribution in the capillary at 3 Torr at a section $y = 0$ at early stages.

4   SUMMARY

The preliminary results of the particles method application to physical processes modeling in a capillary EUV-source of a considered design under the voltage of 23 KV indicate the following.

Electric field blows off free electrons from capillary when the pressure is lower than 2 Torr. Only beam of electrons from the lower volume of the source exists in capillary for a long time.

The region of increased electron density is formed in capillary when the pressure is equal to 2.5 Torr. The region drifts to the exit of the capillary and finds itself in the area at reduced pressure. The peak electron density in the region exceeds 10^{12} 1/cm^3 whereupon the electron bunch is crumbling.

Plasma bunch generation in EUV source becomes possible when the pressure of the gas mixture reaches the value of 3 Torr. The region of increased electron density is formed in the capillary and does not drift. The peak electron density in the region exceeds 10^{13} 1/cm^3 and continues to increase. Subsequent modeling of these processes requires more refined mesh and taking movement of ions into account.

The electron beam, which is generated near the entrance of capillary, plays the role of igniter. It provides the initial conditions for the generation of the region of increased electron density. The ionization intensity sufficient for plasma bunch creation isn't possible without high-energy electrons.

REFERENCES

[1] *Zakharov S.V., Zakharov V.S., Novikov V.G., Mond M., Choi P.* Plasma dynamics in a hollow cathode triggered discharge with the influence of fast electrons on ionization phenomena and EUV emission// IOP PUBLISHING PLASMA SOURCES SCIENCE AND TECHNOLOGY Plasma Sources Sci. Technol. 17 (2008) 024017 (13pp) doi:10.1088/0963-0252/17/2/024017.

[2] *N. F. Mott, H.S.W. Massey.* The Theory of Atomic Collisions. Oxford, Clarendon Press, 1965.

[3] *I.M. Gelfand, G.E. Shilov*. The Generalized Functions and operations with them. (In Russian), Moscow, Dobrosvet Press, 2000.

[4] *A.V. Berezin, A.S. Dukhanin, M.B. Markov, S.V. Parot'kin, A.V. Sysenko, A.S. Vorontsov.* The Electron-Photon Cascade in Gas. Chapter 1. Equations and Approximations of the Model // Keldysh Institute for Applied Mathematics Preprint. 2012. № 6. URL: http://library.keldysh.ru/preprint.asp?id=2012-6.

[5] *Mikhail B. Markov, Mikhail E. Zhukovskiy*. Modeling the radiative electromagnetic field. International Journal of Computing Science and Mathematics 2008 - Vol. 2, No.1/2 pp.110 – 131.

[6] *A.N. Andrianov A.V. Berezin, A.S.Vorontsov, K.N. Efimkin, M.B.Markov*. The Radiation Electromagnetic Fields Modeling at the Multiprocessor Computing Systems. Moscow, Mathematical Modeling, V.20, №3, 2008. P. 98-114.

[7] *A.V. Berezin, A.S.Vorontsov, M.B.Markov, B.D. Plyushchenkov.* On the Conclusion and Solution of Maxwell Equations for the Problems with Given Wavefront. Moscow, Mathematical Modeling, V.18, №4, 2006. P.43-60.

[8] *Weyhreter M. et al.* Measurements of differential cross sections for e-Ar, Kr, Xe scattering at E=0.05 – 2 eV // Z. Phys. D, 1988, No. 7, p. 333.

[9.] *Yuan J. et al.* Quasirelativistic low-energy electron-atom scattering: Xe // J. Phys. B, 1991, Vol. 24, p. 275.

[10] *Gibson C. et al.* Low-energy electron scattering from xenon // J. Phys. B, 1998, Vol. 31, p. 3949.

[11] *Register D. F. et al.* Elastic electron scattering cross sections // J. Phys. B, 1986, Vol. 19, p. 1685.

[12] *Linert I. et al.* Dfferential cross sections for elastic electron scattering in xenon in the energy range from 5 eV to 10 eV // Phys. Rev. A, 2007, Vol. 76, p. 03271.

[13] *Eachran R.P. et al.* Elastic scattering of electrons from krypton and xenon // J. Phys. B, 1984, Vol. 17, p. 2507.

[14] *Nishimura H. et al*. Elastic scattering of electrons from xenon // J. Phys. Soc. Jap., 1987, Vol. 56, No. 1, p. 70.

[15] *Salvat F.* Optical-model potential for electron and positron elastic scattering by atoms // Phys. Rev. A, 2003, Vol. 68, p. 012708.

[16] Official site National Institute of Standarts and Technology – http://www.phys.nist.gov/

[17] Numerical data and functional relationships in science and technology. Group I. Elementary particles, nuclei and atoms. V.17. Photon and electron interactions with atoms, molecules and ions. Subvolum A. Interaction of photon and electron with atoms / Edited by Itikawa Y. – Berlin: Springer, 2000.

[18] *Kim Y.-K., Rudd M.E.* Binary-encounter-dipole model for electron-impact ionization // Phys. Rev. A, 1994, Vol. 50, pp. 3954 – 3967.

[19] *Kim Y.* Extension of the binary-encounter-dipol model to relativistic incident electrons // Phys. Rev. A, 2000, Vol. 62, p. 052710.

[20] *Rapp D., Briglia D.D* Ionization by electron impact II // J. Chem. Phys., 1965, Vol. 43, No. 5, p. 1480.

[21] *Rejoub R. et al.* Determination of the absolute partial and total cross sections for electron-impact ionization of the rare gases // Phys. Rev. A, 2002, Vol. 65, p. 042713.

[22] *A.N. Andrianov A.V. Berezin, A.S.Vorontsov, K.N. Efimkin, V.F. Zintchenko, M.B.Markov, A.M. Tchlenov.* Modeling the Electron Beam from the Accelerator LIA-10 on the Multiprocessor System. Moscow, Mathematical Modeling, V.22, №2, 2010. P. 29-44.

[23] *Bowe J.C.* Drift velocity of electron in Nitrogen, Neon, Argon, Krypton and Xenon // Phys. Rev., 1960, Vol. 117, p. 1411.

[24] *Wagner K. H. //* Z. Phys., 1964, Vol. 178, p. 64.

[25] *Makabe T. et al. //* J. Phys. B, 1978, Vol. 11, p. 3785.

[26] *Hayashi M.* Calculation of swarm parameters in xenon at high E/N by a Monte Carlo simulation method // J. Phys. D, 1983, Vol. 16, p. 591.

[27] *Kruithof A.A. //* Physica, 1940, Vol. 7, p. 519.